



A EUROPEAN JOURNAL OF CHEMICAL BIOLOGY

CHEM **BIO** CHEM

SYNTHETIC BIOLOGY & BIO-NANOTECHNOLOGY

Accepted Article

Title: Substrate recognition and catalytic mechanism of the phosphate acyltransferase PlsX from *Bacillus subtilis*

Authors: Yiping Jiang, Mingming Qin, and Zhihong Guo

This manuscript has been accepted after peer review and appears as an Accepted Article online prior to editing, proofing, and formal publication of the final Version of Record (VoR). This work is currently citable by using the Digital Object Identifier (DOI) given below. The VoR will be published online in Early View as soon as possible and may be different to this Accepted Article as a result of editing. Readers should obtain the VoR from the journal website shown below when it is published to ensure accuracy of information. The authors are responsible for the content of this Accepted Article.

To be cited as: *ChemBioChem* 10.1002/cbic.202000015

Link to VoR: <http://dx.doi.org/10.1002/cbic.202000015>

WILEY-VCH

www.chembiochem.org



Substrate recognition and catalytic mechanism of the phosphate acyltransferase PlsX from *Bacillus subtilis*

Yiping Jiang,^[a] Mingming Qin,^[a] Zhihong Guo^{*[a]}

[a] Dr. Yiping Jiang, Dr. Mingming Qin, and Professor Zhihong Guo
Shenzhen Research Institute, Hong Kong Branch of Guangdong Southern Marine Science and Engineering Laboratory (Guangzhou) and Department of Chemistry
The Hong Kong University of Science and Technology
Clear Water Bay, Kowloon, Hong Kong SAR, China
E-mail: chguo@ust.hk

Abstract: Phosphate: acyl-acyl carrier protein (ACP) acyltransferase PlsX is a peripheral enzyme catalyzing acyl transfer to orthophosphate in phospholipid synthesis. Little is known about how it recognizes substrates and catalyzes the acyl transfer reaction. Here we show that its active site include many residues lining a long narrow gorge at the dimeric interface, two positive residues forming a positive ACP docking pad next to the interfacial gorge, and a number of strictly conserved residues significantly contributing to the catalytic activity. These findings suggest a substrate recognition mode and a catalytic mechanism that is different from phosphotransacetylases catalyzing a similar acyl transfer reaction. The catalytic mechanism involves substrate activation and transition state stabilization by two strictly conserved residues, lysine-184 and asparagine-229. Another noticeable feature of the catalysis is the release of the acyl phosphate product to membrane proximity which may facilitate its membrane insertion.

Introduction

Fatty acids are a major component of phospholipids and are synthesized de novo by the type II fatty acid synthase in bacteria.^[1] They are generated as a thioester of an acyl carrier protein (ACP) that is either directly used in synthesis of phosphatidic acid or converted first to an acyl phosphate through transferring its acyl group to inorganic orthophosphate by a phosphate acyltransferase called PlsX.^[2,3] In a large set of bacteria including many Gram-positive pathogens such as *Staphylococcus aureus* and *Streptococcus pneumoniae*,^[4] PlsX is the only connecting enzyme between fatty acid synthesis and phospholipid synthesis and is an attractive drug target.^[5] Besides its catalytic function, PlsX has been scrutinized for its peripheral localization to membrane, which features a punctate pattern in either fixed cells^[2, 5] or live cells.^[6] These punctate foci are only observed in the early log phase^[7] and have been identified as fluid membrane microdomains termed regions of increased fluidity (RIFs).^[8,9] A short amphipathic α -peptide in the middle of the helix-turn-helix interface of the dimeric enzyme has been found to mediate RIFs localization through modulating its hydrophobic interaction with the fatty acyl moieties of the cytoplasmic membrane leaflet.^[10] Mutations disrupting this membrane association were found to delay transition to the log phase and cause a lower cell density in stationary phase, demonstrating significance of the peripheral localization.^[10,11]

PlsX shares sequence homology with members of the protein family Pfam01515 that includes phosphotransacetylase (Pta) and phosphotransbutyrylase (Ptb), which catalyze the

reversible transfer of an acetyl or butyryl group between orthophosphate and coenzyme A (CoA-SH), respectively. It has not been examined for its catalytic mechanism except simple steady-state kinetic characterization,^[2] but Pta has been mechanistically investigated in depth using both biochemical and structural methods. Early kinetic studies suggested that a ternary complex is involved in the catalysis of *Clostridium kluyveri* Pta,^[12, 13] which is consistent with the failed attempt to detect an acetyl-enzyme intermediate.^[14] In addition, kinetic and mutational analysis of Pta from *Methanosarcina thermophila* identified a nonessential cysteine and three conserved arginine residues at the active site, of which one residue (Arg310) was suggested to be a catalytic residue.^[15, 16] In 2004, the crystal structure of *Methanosarcina thermophila* Pta was determined in its apo form, which features a dimeric architecture containing two α/β domains in a monomer and a potential active site locating at the domain interface.^[17] Subsequently, CoA-SH was successfully soaked into the active site,^[18] revealing its stabilization by hydrogen bonds and hydrophobic interaction by multiple residues including the previously identified arginine residues. Importantly, the soaked crystal structure shows that three residues, namely Ser309, Arg310, and Asp316, are proximal to the sulfhydryl group of the CoA-SH substrate. On this basis, kinetic characterization of site-directed mutants allowed proposal of a catalytic mechanism in which Asp316 serves as a base to deprotonate CoA-SH for the nucleophilic reaction, Arg310 orients and positions the acetyl phosphate substrate, and Ser309 stabilizes the negative charge of transition state by hydrogen bonding. The proposed roles of Ser309 and Arg310 appear to be supported by a Pta-acetyl phosphate complex structure in which their equivalents in the *Bacillus subtilis* enzyme (Ser303 and Arg304) interact directly with the phosphate group of one acetyl phosphate ligand, despite the fact that they make no contact with another acetyl phosphate ligand bound in proximity of the first one.^[19]

Three PlsX crystal structures have been determined for comparison with Pta, two from *Bacillus subtilis*^[10, 20] and one from *Enterococcus faecalis*.^[21] They are all dimeric without a natural ligand and have an $\alpha/\beta/\alpha$ sandwich structure consisting of a twisted β -sheet of 11 mostly parallel strands flanked by 13 helices. Two of the helices ($\alpha 8$ and $\alpha 10$) protrude from the main domain as a long hairpin and form a four-helix bundle at the dimer interface, which contains the amphipathic α -peptide sensor of RIFs.^[10] Structural comparison found that PlsX and Pta are close structural neighbors by DaliLite.^[22] In addition, two large symmetric cavities are found at the PlsX dimer interface, which occupy equivalent positions of the active sites in Pta. However, the catalytic residues (Ser309, Arg310 and Asp316) and other conserved residues in the *M. thermophila* Pta active site find no

FULL PAPER

equivalents in the PlsX cavities, suggesting that the two enzymes likely adopt a different strategy to recognize the substrates for catalysis of the similar acyl transfer reaction.

To understand how PlsX recognizes its substrate and catalyzes the acyl transfer reaction, we used bioinformatics analysis and docking of natural ligands to identify potential active site residues. The suspected residues were then varied by site-directed mutagenesis and the resulting mutant proteins were

characterized for their steady-state kinetics. Based on the assessment of their catalytic contribution, we successfully identified the residues involved in the catalysis and recognition of various moieties of the natural substrates/products including ACP, its phosphopantetheinyl linker, the phosphate group and the acyl group. These results support a PlsX catalytic mechanism that is different from that of phosphotransacetylases.

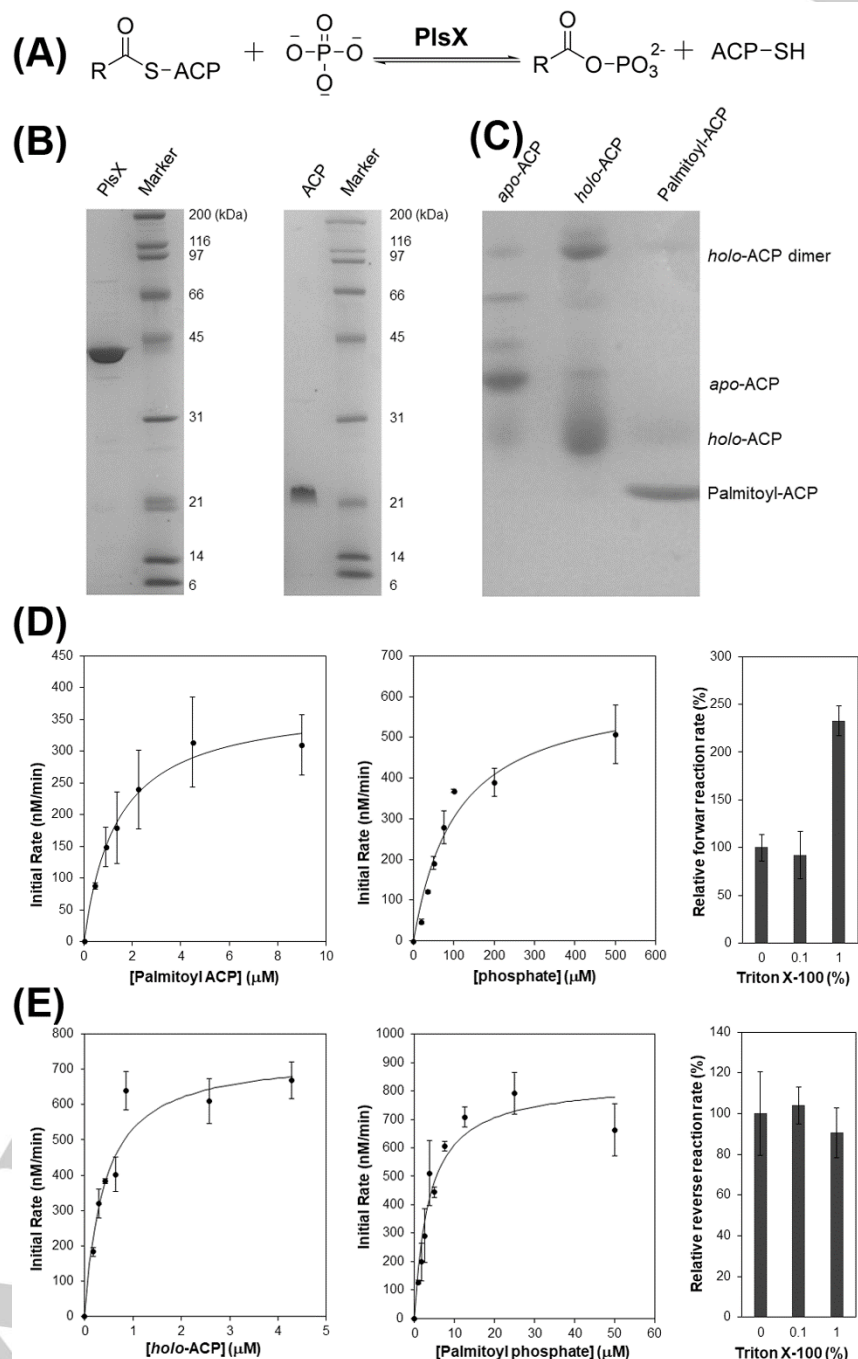


Figure 1. Steady-state kinetics of PlsX. (A) The reversible reaction catalysed by PlsX. (B) Reductive SDS-PAGE of the purified PlsX and ACP (*apo* form). *apo*-ACP has a calculated molecular weight of 8.5 kDa and shows an abnormal mobility due to its low binding affinity for SDS. (C) UREA-PAGE of *apo*-ACP and its derivatives. Both *holo*-ACP and palmitoyl-ACP were purified after preparation. (D) Michaelis-Menten kinetics of the forward reaction and Triton X-100 effect on the reaction rate. (E) Michaelis-Menten kinetics of the reverse reaction and Triton X-100 effect on the reaction rate. See experimental section for the detailed conditions in the determination of the steady-state kinetics. In (D) and (E), the solid lines are curve-fitting results using the Michaelis-Menten equation. Effects of Triton X-100 were determined at saturating substrate concentrations: 10 μM palmitoyl-ACP and 500 μM phosphate for the forward reaction and 5 μM *holo*-ACP and 20 μM palmitoyl phosphate for the reverse reaction.

FULL PAPER

Results and Discussion

Steady-state kinetic characterization

Using radiolabeled substrates, *Streptococcus pneumoniae* PlsX has been shown to catalyze both the forward and reverse transfer of palmitoyl group between ACP and orthophosphate (Figure 1A).^[2] For the forward reaction, the enzyme is specific for palmitoyl-ACP with no activity for palmitoyl-CoA and has a K_M value of 300 μM and 140 μM for palmitoyl-ACP and orthophosphate, respectively. To better correlate the kinetic properties to crystal structures, we characterized the steady-state kinetics of *Bacillus subtilis* PlsX, which shares 52.9% sequence identity with the *Streptococcus pneumoniae* orthologue and has had its structure determined to high resolution.^[10, 20] The protein was overexpressed in *E. coli* with a C-terminal hexahistidine tag and successfully purified to homogeneity (Figure 1B). apo-ACP (8.5 kDa) from *Bacillus subtilis* was also prepared and purified to homogeneity, which showed an abnormal mobility on SDS-PAGE (~25 kDa, Figure 1B) due to its low binding affinity of the detergent.^[23] *holo*-ACP and palmitoyl-ACP were subsequently prepared from apo-ACP (Figure 1C) and used as substrates together with palmitoyl phosphate or phosphate in the kinetic characterization. The enzymic reaction was found to conform to the Michaelis-Menten equation in both forward (Figure 1D) and reverse (Figure 1E) reactions. For the forward reaction, K_M is 1.4 μM and 104 μM and k_{cat} is 0.76 min^{-1} and 0.62 min^{-1} for palmitoyl-ACP and orthophosphate, respectively; while for the reverse reaction, K_M is 0.39 μM and 3.7 μM and k_{cat} is 148 min^{-1} and 167 min^{-1} for *holo*-ACP and palmitoyl phosphate, respectively (Table 1). These kinetic data show that the reverse reaction is more than 200 time faster than the forward reaction under saturation conditions and the enzyme's catalytic efficiency (k_{cat}/K_M) is the highest for *holo*-ACP with a value of $6.3 \times 10^6 \text{ M}^{-1} \cdot \text{s}^{-1}$. Considering the fact that PlsX is a membrane protein,^[5-8, 10] the neutral detergent Triton X-100 was added to the enzymic reaction and found to more than double the forward reaction rate at a high concentration of 1% but have no effect at a lower concentration of 0.1% (Figure 1D). However, this detergent had no effect on the reverse reaction even at the high concentration (Figure 1E).

Table 1. Kinetics constant of *Bacillus subtilis* PlsX.

Substrate	k_{cat} (min^{-1})	K_M (μM)
Palmitoyl-ACP	0.76 ± 0.08	1.4 ± 0.4
Phosphate	0.62 ± 0.05	104 ± 19
<i>holo</i> -ACP	148 ± 8	0.39 ± 0.07
Palmitoyl phosphate	167 ± 10	3.7 ± 0.7

For the forward reaction, *Bacillus subtilis* PlsX exhibits a much higher affinity (lower K_M) for palmitoyl-ACP than *Streptococcus pneumoniae* PlsX, demonstrating that it has a much higher activity. There are two probable contributors to this high activity of the *Bacillus* enzyme. One important factor is the use of ACP from the same bacterial strain in the current study, whereas the source of ACP was not specified in the previous study.^[2] Another factor is the current use of real time measurement of the rate, which was completed before the

reverse reaction became significant enough to affect the measurement accuracy. In contrast, the rate measurement took a much longer time in the previous study,^[2] which should be significantly affected by the reverse reaction in consideration of the fact that the reverse reaction is much faster than the forward reaction. Taking these factors into consideration, PlsX is likely to have a much higher activity as determined for the *Bacillus subtilis* orthologue in this study.

Docking simulation

To understand how PlsX interacts with its substrates, the natural ligands or their analogs were docked to the suspected active site cavity using AutoDock.^[24] Palmitoyl phosphate, a product of the forward reaction and a substrate of the reverse reaction, was first successfully docked at a long channel formed by both subunits of the enzyme. The docked ligand is shown in Figure 2A with all contact residues, of which most are from $\alpha 8$, the $\beta 7$ -to- $\alpha 6$ loop and the $\beta 8$ -to- $\alpha 7$ loop from the other monomer. Its alkyl chain binds in a twisted conformation to the lower part of the interfacial channel, whereas the carboxyl phosphate head group binds in the upper part. Interestingly, the alkyl chain interacts favorably with hydrophobic side chain residues that form a tortuous open channel, while the polar head group is stabilized by

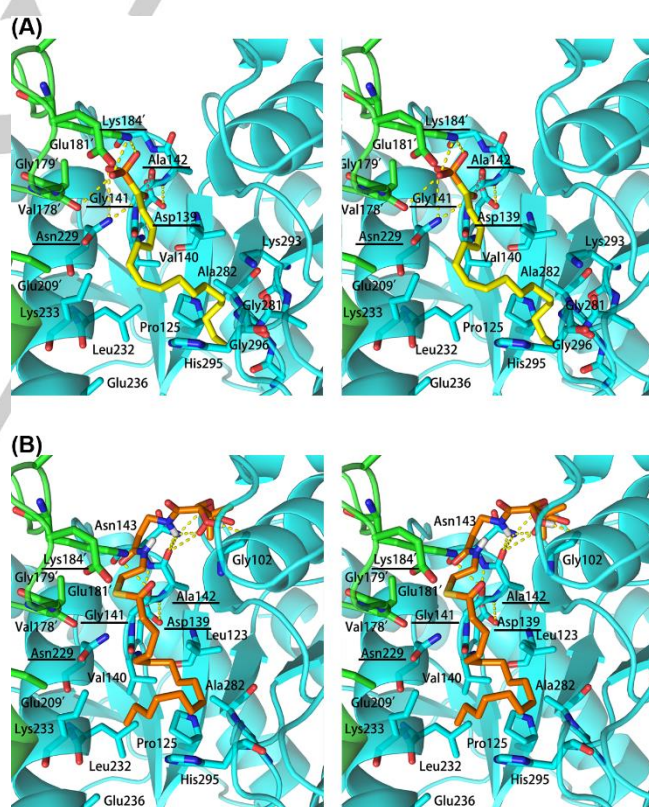


Figure 2. Docking of ligands to the active site of PlsX. (A) Stereo diagram of the active site with the docked palmitoyl phosphate. (B) Stereo diagram of the active site with the docked palmitoyl 4'-phosphopantetheinyl thioester. The protein is represented in cartoon and colored according to subunit with active site residues in sticks, while palmitoyl phosphate and palmitoyl 4'-phosphopantetheinyl thioester are represented in yellow and brown sticks, respectively. Underlined residues interact with polar head group of palmitoyl phosphate and likely play important roles in the catalysis. Gold dashed lines denote hydrogen bonds with a distance $\leq 3.6 \text{ \AA}$ and the grey dashed line in (A) indicates a short distance of 2.9 \AA . Amino acid residues from a different subunit are labeled with a primed number.

FULL PAPER

ionic interactions and multiple hydrogen bonds. The carboxyl oxygen atom of the acyl group is within a hydrogen-bonding distance of 3.0 Å to the amide nitrogen atom in the sidechain of Asn229 in $\alpha 8$ and is interestingly close to the backbone carbonyl oxygen atom of Gly141 at a distance of 2.9 Å, which is apparently positioned by a hydrogen bond between its α -N and the sidechain carboxylate of Asp139 in the $\beta 7$ -to- $\alpha 6$ loop. The phosphoryl group is mainly stabilized by residues in the loop connecting $\beta 8$ to $\alpha 7$ from the other monomer, forming two ionic hydrogen bonds with the sidechain ammonium ion of Lys184' and one hydrogen bond with the backbone carbonyl group of Val178'. It is also close to the side chain amide of Asn229 with a distance of 3.6 Å.

Palmitoyl 4'-phosphopantetheinyl thioester, a surrogate of the palmitoyl-ACP substrate in the forward reaction, was also successfully docked to the large cavity at the PlsX dimeric interface with a similar orientation as palmitoyl phosphate (Figure 2B). Its acyl chain takes an alternative twisted conformation but its carbonyl group makes similar contacts with Asn229, Lys184' and Gly141 in comparison to the acyl group of the docked palmitoyl phosphate. Interestingly, the positive side chains of Arg73 and Arg120 are located at the edge of the cavity at a short distance of less than 7 Å from the 4'-phosphoryl group of the docked ligand (Figure 3). These residues, together with nearby positive residues such as Arg70, Arg114 and Lys183' on the protein surface (Figure 3), may form a docking pad for recognition of the negatively charged $\alpha 2$ -helix of ACP,^[25-27] similar to those found on acyl-ACP hydrolases such as BioW and BioH from the biotin biosynthetic pathway.^[28, 29] Thus, this docking simulation gives rise to a model for the binding of palmitoyl-ACP in which the ACP moiety docks to the positively charged pad at the edge of the interfacial cavity and allows the palmitoyl 4'-phosphopantetheinyl thioester moiety to bind the full length of the long channel at the dimer interface in a largely extended conformation. Such a binding model is consistent with another recent structural modeling of the substrates to PlsX.^[11]

Conservation of potential active site residues

To understand whether the identified amino acid residues in

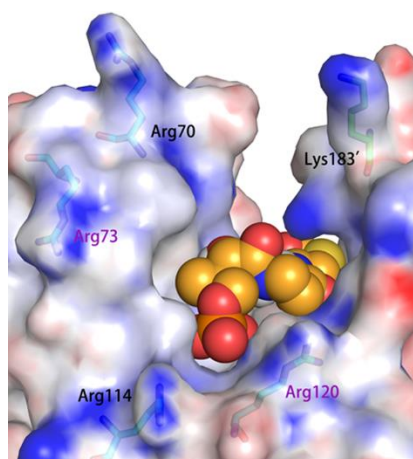


Figure 3. The identified ACP docking pad. It is viewed along the axis of the active site channel between the two subunits and is comprised of conserved Arg73 and Arg120 labeled in purple. Other positive residues (labeled in black) are not conserved. PlsX is represented in electron potential surface with all positive residues in sticks, while the docked palmitoyl 4'-phosphopantetheinyl thioester is represented in ball and stick with brown carbon atoms and only part of the 4'-phosphopantetheinyl group is visible.

the docking simulation are conserved, all reviewed PlsX sequences in the UniProt database were withdrawn and filtered at 50% sequence identity to obtain 95 non-redundant sequences for multiple sequence alignment. A total of 13 amino acid residues were found to be absolutely conserved, of which ten residues are located in the long $\alpha 8$ helix, the $\beta 7$ -to- $\alpha 6$ loop and the $\beta 8$ -to- $\alpha 7$ loop from the other subunit (Figure 2 and Figure 4). The other three residues include Gly99, Gly207' and Glu209', of which the last two are close to the active site channel as shown in Figure 2. Besides these strictly conserved residues, many other residues forming the interfacial cavity are also conserved, including the few residues interacting with the 4'-phosphoryl group of the docked palmitoyl 4'-phosphopantetheinyl thioester (Figure 2) and the residues that form most of the large hydrophobic pocket for the acyl chain in two orientations (Figure 2A and Figure 2B). In addition, Arg73 and Arg120 of the suspected ACP docking pad (Figure 3) are replaced by lysine residues in a few orthologues and are thus also highly conserved. However, the other suspected positive residues, namely Arg70, Arg114 and Lys183', are not conserved at all and are thus very unlikely to be part of the docking pad.

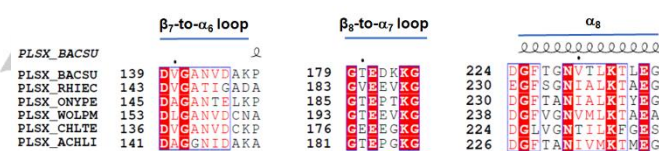


Figure 4. Strictly conserved amino acid residues at the active site of PlsX. The residues shaded in red are strictly conserved among 95 reviewed PlsX sequences filtered at 50% sequence identity from the UniProt database. The aligned sequences are selected from these PlsX orthologues and named directly with their UniProtKB mnemonic identifiers. The aligned secondary structures are from the *Bacillus subtilis* PlsX structure (PDB ID: 6A1K).

Active site mutants and their kinetic properties

To test the veracity of the docking models, site-directed mutagenesis was used to assess the contribution of key amino acid residues to enzyme catalysis. The strictly conserved non-glycine residues in direct contact with the docked ligands including Lys184, Asn229, Lys233 and Glu236, were each mutated to alanine. Lys184 was additionally mutated to arginine or glutamine and Asn228 was additionally mutated to glutamine because either residue interacts with the key functionalities in the docked palmitoyl phosphate (Figure 2A). In addition, the strictly conserved residues in proximity of the direct-contact residues, including Glu181 and Glu209, were also individually mutated to alanine. Moreover, the conserved positive residues of the suspected ACP docking site, Arg73 and Arg120, were mutated into alanine, while the non-conserved Arg114 in proximity was also mutated to alanine as a negative control. A double mutant with both Arg73 and Arg120 mutated to alanine, R73A/R120A, was also constructed. All these mutation proteins were overexpressed to a high level and were readily purified to homogeneity like the hexahistidine-tagged wild-type PlsX. Analysis by circular dichroism spectroscopy showed no difference between these mutant proteins and the wild-type protein, indicative of negligible effect of the point mutations on the overall structure of PlsX.

The steady-state kinetic constants, k_{cat} and K_M , were determined for the forward reaction for the mutant proteins. As

FULL PAPER

Table 2. Kinetic constants of PlsX mutant proteins in the forward reaction.

Protein	Substrate	k_{cat} (min ⁻¹)	$k_{cat}(wt)/k_{cat}$	K_M (μM)	$K_M/K_M(wt)$	k_{cat}/K_M (M·min ⁻¹)	$[k_{cat}/K_M](wt)/k_{cat}/K_M$
WT	Palmitoyl-ACP	0.76 ± 0.08	1.0	1.37 ± 0.42	1.0	(5.6 ± 3.1) × 10 ⁵	1.0
	Phosphate	0.62 ± 0.05	1.0	104 ± 19	1.0	(6.0 ± 1.9) × 10 ³	1.0
R73A	Palmitoyl-ACP	0.85 ± 0.06	0.89	4.50 ± 0.46	3.28	(1.9 ± 0.4) × 10 ⁵	2.9
	Phosphate	0.72 ± 0.04	0.86	111 ± 21	1.07	(6.5 ± 2.0) × 10 ³	0.92
R114A	Palmitoyl-ACP	0.72 ± 0.04	1.06	1.70 ± 0.35	1.24	(4.2 ± 1.4) × 10 ⁵	1.3
	Phosphate	0.73 ± 0.04	0.85	127 ± 23	1.22	(5.7 ± 1.7) × 10 ³	1.1
R120A	Palmitoyl-ACP	0.77 ± 0.03	0.99	3.36 ± 0.34	2.45	(2.3 ± 0.4) × 10 ⁵	2.4
	Phosphate	0.74 ± 0.03	0.84	131 ± 21	1.26	(5.6 ± 1.4) × 10 ³	1.1
R73A/ R120A	Palmitoyl-ACP	nd ^a	--	nd	--	nd	--
	Phosphate	nd	--	nd	--	nd	--
E181A	Palmitoyl-ACP	0.27 ± 0.02	2.81	1.35 ± 0.20	0.99	(2.0 ± 0.4) × 10 ⁵	2.8
	Phosphate	0.26 ± 0.01	2.38	239 ± 37	2.30	(1.8 ± 0.3) × 10 ³	3.3
K184A	Palmitoyl-ACP	0.12 ± 0.01	6.33	1.49 ± 0.32	1.09	(8.1 ± 3.1) × 10 ⁴	6.9
	Phosphate	0.14 ± 0.01	4.43	802 ± 137	7.71	(1.7 ± 0.5) × 10 ²	35.3
K184Q	Palmitoyl-ACP	0.15 ± 0.01	5.00	2.02 ± 0.46	1.47	(7.4 ± 2.8) × 10 ⁴	7.6
	Phosphate	0.17 ± 0.01	3.65	425 ± 59	4.09	(4.0 ± 0.9) × 10 ²	15.0
K184R	Palmitoyl-ACP	0.40 ± 0.02	1.90	1.39 ± 0.20	1.01	(2.9 ± 0.7) × 10 ⁵	1.9
	Phosphate	0.41 ± 0.02	1.51	52 ± 8	0.50	(7.9 ± 1.9) × 10 ³	0.76
E209A	Palmitoyl-ACP	0.22 ± 0.02	3.45	1.24 ± 0.24	0.91	(1.8 ± 0.6) × 10 ⁵	3.1
	Phosphate	0.20 ± 0.02	3.10	93 ± 14	0.89	(2.2 ± 0.6) × 10 ³	2.7
N229A	Palmitoyl-ACP	0.06 ± 0.01	12.7	6.00 ± 0.86	4.38	(1.0 ± 0.4) × 10 ⁴	56.0
	Phosphate	0.06 ± 0.01	10.3	267 ± 60	2.57	(2.2 ± 1.1) × 10 ²	27.3
N229Q	Palmitoyl-ACP	0.87 ± 0.08	0.87	3.04 ± 0.41	2.22	(2.9 ± 0.8) × 10 ⁵	1.9
	Phosphate	0.75 ± 0.05	0.83	126 ± 25	1.21	(6.0 ± 2.0) × 10 ³	1.0
K233A	Palmitoyl-ACP	0.18 ± 0.01	4.22	1.43 ± 0.24	1.04	(1.3 ± 0.3) × 10 ⁵	4.3
	Phosphate	0.20 ± 0.02	3.10	136 ± 18	1.31	(1.5 ± 0.4) × 10 ³	4.0
E236A	Palmitoyl-ACP	0.25 ± 0.02	3.04	1.08 ± 0.22	0.79	(2.3 ± 0.8) × 10 ⁵	2.4
	Phosphate	0.27 ± 0.01	2.30	151 ± 18	1.45	(1.8 ± 0.3) × 10 ³	3.3

[a] nd: not detected; no activity was detected with 1-10 μM mutant enzyme, 2-30 μM palmitoyl-ACP and 0.5-2 mM phosphate.

shown in Table 2, the catalytic activity of the negative control mutant protein R114A is essentially the same as the wild-type protein for both substrates. In comparison, R73A and R120A cause a significant 2.5~3.3-fold increase in K_M for palmitoyl-ACP without adverse effect on other kinetic constants, whereas double mutations (R73A/R120A) diminish the activity to an undetectable level even when measured at an increased concentration for the protein and the substrates. This pattern of activity change is consistent with those observed for known ACP docking pads, for which removal of one positive residue leads to only mild decrease in activity whilst removal of all positive residues causes severe activity loss.^[28, 29] Among the remaining mutations, N229A causes the greatest k_{cat} decrease by more than 10 fold and increases K_M by 4.4 and 2.6 fold for palmitoyl-ACP and phosphate, respectively. However, most of the catalytic activity is recovered with a 2.2-fold K_M increase for palmitoyl-ACP when glutamine is introduced into the mutated position (in N229Q). These kinetic changes strongly suggest an important role of the Asn229 side chain in stabilizing the transition state and are fully consistent with its simultaneous interaction with the carboxyl oxygen and phosphoryl group of the

docked palmitoyl phosphate (Figure 2A). In contrast, K184A causes the greatest K_M increase of 7.7 fold for phosphate with no K_M effect on the other substrate and also a significant 4.4~6.3 fold k_{cat} decrease. The damage in catalytic activity remains little changed when a glutamine is used to replace the strictly conserved Lys184 (in K184Q), but the activity is basically recovered with a mild ~2-fold k_{cat} decrease when an arginine is introduced into the mutated position (in K184R). Consistent with the docking results (Figure 2), these mutational results support a crucial role of Lys184 in binding of the phosphate substrate and in stabilizing the transition state. Finally, E181A is another mutant protein that exhibits a significant 2.3-fold K_M increase for phosphate without affecting the other substrate, suggesting that Glu181 also contributes to binding of phosphate. The remaining mutant proteins including E209A, K233A and E236A are similar to the wild-type protein in K_M for both substrates, but exhibit a modest 2-4 fold k_{cat} decrease like E181A. Taken together, results from these kinetic studies strongly support the interactions between the ligands and the conserved active site residues identified in the docking simulations (Figure 2), although the

FULL PAPER

kinetic parameters of the mutant proteins were not determined for the reverse reaction due to the chemical instability of palmitoyl phosphate.

Substrate recognition

The modeling and mutational results reveal the mode of substrate recognition of PlsX in which acyl-ACP is recognized by multiple-pronged interactions spread throughout its structure (Figure 5). Its ACP moiety is recognized by the ionic interactions

with the positive docking pad consisting of two conserved residues Arg73 and Arg120 and a few hydrogen bonds at the 4'-phosphoryl group and the pantothenate carbonyl (with the Gly141 backbone, Figure 2B). Meanwhile, its acyl carbonyl is likely stabilized by a hydrogen bond with the side chain of Asn229 as supported by a similar hydrogen bond for the docked palmitoyl phosphate (Figure 2A) and a significant K_M increase for the substrate caused by the N229A mutation (Table 2). Moreover, the acyl group of this substrate is stabilized by many hydrophobic

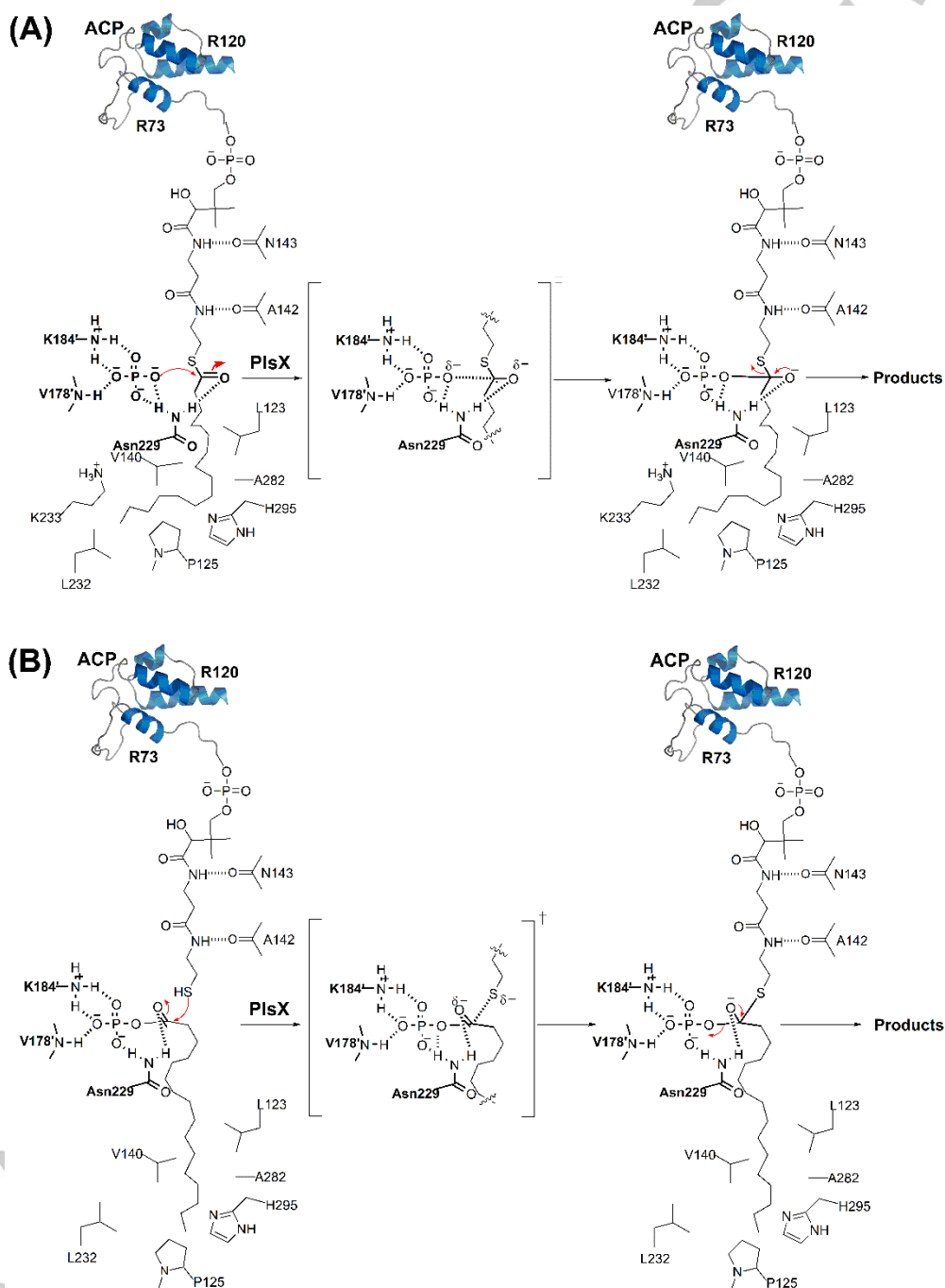


Figure 5. Proposed catalytic mechanism for PlsX. (A) The reaction mechanism of the forward reaction. (B) The reaction mechanism of the reverse reaction.

FULL PAPER

side chains lining the binding channel (Figure 2B). The multiplicity of the interactions and their balanced distribution throughout the full length of the substrate ensure the high substrate specificity. However, this multivalent mode of substrate recognition implies that any individual binding residue contributes only a limited portion to the overall binding energy. In consistence with this binding mode, only moderate K_M increase of 4.4-fold or less is found for any single point mutation (Table 2). This multivalent binding mode may also underlie the fact that only two conserved positive residues form the ACP docking pad, while at least three such residues are involved in other ACP-binding proteins such as BioH and BioW.^[28, 29]

The other substrate, phosphate, is recognized mostly by the highly conserved $\beta 8$ -to- $\alpha 7$ loop from the other subunit through two ionic hydrogen bonds with Lys184' and one neutral hydrogen bond with the backbone amide of Val178', like the binding of the phosphoryl group of the docked palmitoyl phosphate (Figure 2A). Glu181' of this loop also contributes to phosphate binding as indicated by the significant increase in K_M for E181A (Table 2). This residue may directly interact with the substrate through hydrogen bonding or may interact with the Lys184' side chain to orient it for optimal interaction with the substrate. In addition, Asn229 also contributes to phosphate binding as suggested by its hydrogen bonding with the phosphate group of the docked palmitoyl phosphate (Figure 2A) and by the significant K_M increase for N229A (Table 2). Since the Asn229 side chain also interacts with the other substrate, this residue likely couples the phosphate binding to the binding of acyl-ACP. This potential coupling suggests that the phosphate binding site is fully formed only after binding of acyl-ACP. In the phosphate binding, Lys184' likely plays a dominant role as suggested by the largest K_M increase for its alanine mutant (Table 2).

Catalytic mechanism

After active site binding, acyl-ACP and phosphate are well positioned for the acyl transfer from ACP to phosphate through a nucleophilic addition reaction. The transition state is likely stabilized by the side-chain amide of Asn229, the Lys184' side chain and the backbone amide of Val178' (Figure 5A). In addition, the strictly conserved Glu181' may also contribute to this transition state stabilization either directly through interaction with phosphate or indirectly through interacting with the proximal Lys184'. The catalytic roles of these residues are consistent with the significant k_{cat} decrease for the corresponding site-directed mutant proteins, particularly for N299A (Table 2).

The same set of the binding and catalytic residues are also suitable for binding the substrates of the reverse reaction and efficiently catalyzing their reaction (Figure 5B). Specifically, the palmitoyl phosphate substrate is tightly bound to the active site by the polar interactions (with Asn229, Glu184' and the backbone amide of Val178') and the hydrophobic interactions for the acyl group, while *holo*-ACP is bound to the active site through the interactions at the docking pad and the 4'-phosphoryl group and pantothenate carbonyl in the prosthetic group. These binding interactions are consistent with the docking results (Figure 2) that are supported by kinetics of the site-directed mutant proteins. Again, the bound substrates are well aligned for nucleophilic attack of the thiol group of *holo*-ACP on the carbonyl group of palmitoyl phosphate, going through a similar transition state that is stabilized by the same conserved residues as for the forward

reaction. Finally, the products are formed from the resulting tetrahedral intermediate through a low barrier collapsing reaction.

In both forward and reverse reactions catalyzed by PlsX, Asn229 plays the most important catalytic role by activating the electrophile and stabilizing the transition state as well as serving the oxyanion hole to stabilize the tetrahedral oxyanion intermediate. No equivalent residue can be found in *Methanosarcina thermophila* Pta that was proposed to use a conserved serine (Ser309) to stabilize the oxyanionic tetrahedral intermediate.^[18] The proposed activation of the thiol substrate by a conserved aspartate (Asp316) in Pta is another mechanistic difference from PlsX, which has no apparent activation mechanism for the thiol substrate and most likely uses a water molecule to deprotonate the thiol group. Nevertheless, both PlsX and Pta use a conserved positive residue to bind the acyl phosphate substrate, namely Lys184' in the former and Arg310 in the latter, although this residue takes a totally different position in the structure of the proteins (Figure 6). This comparison clearly shows that PlsX uses a very different set of amino acid residues to accomplish the similar acyl transfer reaction through a distinct catalytic strategy (Figure 6).

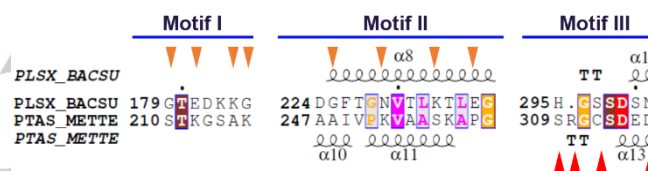


Figure 6. Comparison of key active site residues distributed in three structural motifs in *Bacillus subtilis* PlsX and *Methanosarcina thermophila* phosphotransacetylase (Pta). Catalytic residues in PlsX are indicated by brown triangles while those in Pta are indicated by red triangles. The sequences of the two proteins are aligned with the secondary structure in their corresponding crystal structures (PlsX PDB ID: 6A1K and Pta PDB ID: 2AF4).

Conclusion

In summary, we have successfully identified the active site of PlsX that allows the acyl-ACP product from the fatty acid biosynthetic pathway to dock on protein surface facing the cytosol, with its prosthetic phosphopantetheinyl and the attached acyl chain to bind vertically and linearly in a long and narrow interfacial channel all the way down to the other side of the protein facing plasma membrane. This mode of interaction facilitates not only the binding of the acyl-ACP substrate from the cytosol and release of the ACP product after acyl transfer to the cytosol, but also likely the insertion of the acyl phosphate product into cell membrane where it is used to synthesize phosphatidic acid precursor of phospholipids. In catalysis of PlsX, a strictly conserved asparagine (Asn229) plays a dual role of activating the electrophilic substrate and stabilizing the transition state of the acyl transfer reactions in a mechanism distinct from the structurally homologous Pta^[18] or other bacterial acyltransferases.^[30] These findings for the first time establish the catalytic mechanism of PlsX as a representative peripheral acyl transferase and allow better understanding of the first chemical step of the biosynthesis of phospholipids in most bacteria.

Experimental Section

FULL PAPER

Synthesis of palmitoyl-phosphate and palmitoyl-CoA. Palmitoyl-phosphate was synthesized according to a reported method with minor modifications.^[2, 31] Briefly, 1.20 mmol silver phosphate and 12.25 mmol anhydrous phosphoric acid were dissolved in 10 ml dry diethyl ether and stirred at room temperature for 15 h. Palmitoyl chloride (2.90 mmol) dissolved in 5 ml diethyl ether was added dropwise and the reaction mixture was stirred at room temperature for 1.5 h. After filtering and washing the precipitate twice with 5 ml ethyl ester, the palmitoyl phosphate product in the filtrate was removed off the solvent by rotavaporation. The product was then re-dissolved in 2 ml warm benzene and was recrystallized by cooling to room temperature. After removal of benzene by filtration, the resulting white crystals were washed once with cold benzene and dried *in vacuo*. The final isolated yield of palmitoyl phosphate was 1.5%. ¹H NMR (CD₃OD, 400 MHz): δ 0.92 (t, $J = 6.0$ Hz, 3 H), 1.31 (s, 25 H), 1.65 (m, 2 H), 2.46 (t, 2 H, $J = 7.0$ Hz).

Palmitoyl-CoA was also synthesized with previously reported methods with modifications.^[32-35] In the synthesis, 25 mg CoA-SH (Sigma) was dissolved in 10 ml THF-H₂O solution (v/v, 7:3) and the resulting solution was adjusted to pH = 8.0 by sodium hydroxide, added 50 μ l of palmitoyl chloride, and then stirred for 1.5 h. The reaction mixture was kept at pH 7-8 by adding sodium hydroxide during the reaction. After the reaction, the mixture was removed of THF by rotavaporation and centrifuged at 15,000 g for 2 min to obtain aqueous supernatant, which was collected and added 200 μ l 10% HClO₄ to precipitate the palmitoyl-CoA product as white solid. The precipitated product was collected by centrifugation at 15,000 g for 2 min and washed twice with cold diethyl ether before being dried *in vacuo*. The final isolated yield of palmitoyl-CoA was 45%. Identity of the product was confirmed through comparison with commercial palmitoyl-CoA (Sigma) by its retention factor on silica thin-layer chromatography plates and mass spectrometry (ESI MS: $m/z = 1028$ [M + Na]⁺).

Preparation of holo-ACP and palmitoyl-ACP. Apo-ACP from *Bacillus subtilis* was expressed as a C-terminal fusion of the protein Gb1 with a N-terminal hexahistidine tag and a HRV protease 3C cleavable linker in *E. coli* BL21 (DE3) transformed with a plasmid from laboratory stock. For protein expression, the recombinant cells were streaked on LB agar plates supplemented with 100 μ g/ml ampicillin and incubated at 37°C overnight. Next day, a single colony was picked to inoculate 10 ml Luria-Bertani broth (LB) containing 100 μ g/ml ampicillin and grown overnight at 37°C with shaking at 250 rpm to give a starter culture. The starter culture was used to inoculate 4 L LB medium supplemented with 100 μ g/ml ampicillin and the cells were grown at 37°C with shaking at 250 rpm until OD₆₀₀ reached 0.8-1.0. Then isopropyl- β -D-thiogalactopyranoside (IPTG) was added to a final concentration of 0.2 mM to induce protein expression at 37°C for 3 h. The cell culture was cooled on ice and the cells were harvested by centrifugation and washed once with ice-cold TE buffer (10 mM Tris.HCl, pH 8.0, 1 mM EDTA). The harvested cells were then re-suspended in the start buffer (20 mM Tris.HCl, pH 8.0, 500 mM NaCl, 20 mM imidazole, 10% glycerol) and lysed by sonication. The cell lysate was centrifuged at 30,000 g for 15 min to remove cell debris and the supernatant was loaded onto a 5 ml HisTrap HP column (GE Healthcare) pre-equilibrated with the start buffer. The column was washed by 50 ml start buffer and Gb1-ACP was eluted in ~20 ml 20 mM Tris.HCl buffer (pH 8.0) containing 500 mM NaCl, 200 mM imidazole, and 10% glycerol. The eluted protein solution was concentrated with Amicon® Ultra 15 mL Centrifugal Filters (3 kDa, Millipore) and was desalted into the storage buffer (20 mM Tris pH8.0, 150 mM NaCl) using a HiPrep 26/10 desalting column (GE Healthcare). Subsequently, the desalted protein solution was added 100 μ l 8 mg/ml HRV protease 3C with C-terminal hexahistidine tag from laboratory stock, incubated at 25°C for 1 h, and reloaded onto 5 ml HisTrap HP column (GE Healthcare) pre-equilibrated with storage buffer. ACP was collected from the earliest fractions, concentrated to 28 mg/ml using Amicon® Ultra 15 mL Centrifugal Filters (3 kDa, Millipore), and flash-cooled by liquid nitrogen for storage at -20°C. Protein purity was over 95% examined by SDS-PAGE and densitometry analysis. However, using Urea Polyacrylamide Gel Electrophoresis (UREA-PAGE),^[36-39] the resulting protein solution was found to contain apo-ACP as a major component and to also contain holo-ACP and oxidized holo-ACP dimer as minor components.

Holo-ACP and palmitoyl-ACP were prepared from apo-ACP using the 4'-phosphopantetheinyl transferase Sfp, which was expressed and purified as described previously.^[40, 41] Following a previously reported method,^[42] palmitoyl-ACP was formed from a mixture of 240 μ M apo-ACP, 500 μ M palmitoyl-CoA, 3.4 μ M Sfp, 1 mM MgCl₂, 150 mM NaCl in 50 mM MES (2-(N-morpholino) ethanesulfonic acid) at pH 6.0. The reaction mixture was incubated at 37°C for 4 h and then at room temperature overnight to increase yield and to oxidize holo-ACP to its dimeric form. In this step, almost all apo-ACP was converted to palmitoyl-ACP and most holo-ACP was converted to a dimer as examined by UREA-PAGE. The reaction solution was concentrated with Amicon® Ultra 4 mL Centrifugal Filters (3 kDa, Millipore) and further purified by Superdex-200 10/30 gel filtration column (GE Healthcare) pre-equilibrated with the buffer containing 20 mM Tris, pH 8.0 and 150 mM NaCl. The eluted protein was collected and concentrated to 4 mg/ml, flash-frozen in liquid nitrogen and stored at -20°C. The concentration of the protein was determined by measuring the UV absorbance at 280 nm using an extinction coefficient of 1490 M⁻¹ cm⁻¹ calculated with ProtParam.^[43] The purity of the isolated palmitoyl-ACP was over 90% as estimated from UREA-PAGE and densitometry analysis.

Similarly, holo-ACP was prepared by mixing 500 μ M ACP, 1 mM CoA-SH and 10 μ M Sfp in the buffer containing 50 mM MES (2-(N-morpholino) ethanesulfonic acid) pH 6.0, 10 mM MgCl₂ and 150 mM NaCl. After incubation at 37°C for 4 h, the reaction mixture was loaded onto a 5 ml HisTrap HP column (GE Healthcare) that was pre-equilibrated with the start buffer (20 mM Tris.HCl, pH 8.0, 500 mM NaCl, 20 mM imidazole and 10% glycerol) and eluted out by the same buffer to remove Sfp. Subsequently, the eluted protein solution was concentrated with Millipore YM-3 and further purified by HiPrep 26/10 desalting column (GE Healthcare) that was pre-equilibrated with the storage buffer (20 mM Tris, pH 8.0, 150 mM NaCl and 10% glycerol). The purified holo-ACP was collected and concentrated to 8 mg/ml, flash cooled by liquid nitrogen and stored at -20°C. Protein purity was over 85% examined by UREA-PAGE and densitometry analysis. Since holo-ACP was easily oxidized to its dimeric form, 1 mM dithiothreitol (DTT) was added to the stock solution prior to use.

Preparation and activity assay of PlsX and its mutants. A previously reported procedure was followed exactly to express and purify *B. subtilis* PlsX.^[10] The expression plasmid in the pET28a vector (Novagen) was used as the template for mutation using the QuikChange II XL site-directed mutagenesis kit (Agilent) and the primers listed in Table 3. For production of the double mutant, the R73A-expressing plasmid was used as the template for introducing the second mutation, R120A, into the *plsX* gene. The sequence of the mutated codon and the rest of the gene was verified with full-length DNA sequencing by Beijing Genomics Institute (BGI, Shenzhen, China). The resulting plasmids were transformed into *E. coli* C43 (DE3) (Lucigen) and the resulting cells were used for expression and purification of the mutant proteins exactly like the wild-type PlsX. The proteins were stored until use at -20°C in 10 mM HEPES, pH 7.5, 150 mM NaCl, and 10% glycerol. Oligodeoxynucleotide primers used in the site-directed mutagenesis are listed in Table 3.

The activity of PlsX or its mutant for the forward reaction was determined by measuring the release of free coenzyme A through coupling with the Ellman's Reagent (5,5'-dithio-bis-(2-nitrobenzoic acid) or DTNB).^[44] A typical assay reaction contained 0.5-1.0 μ M PlsX, 500 μ M DTNB, 1 mM MgCl₂, and phosphate and palmitoyl-ACP at varied concentrations in 50 mM Tris pH 7.5. The enzyme was added last to initiate the reaction for real-time monitoring of the formation of 2-nitro-5-thiobenzoate (TNB) by its UV absorbance at 412 nm with an extinction coefficient of 14,150 M⁻¹ cm⁻¹.^[45] Under these conditions, the coupling reaction was tested to be significantly faster than the enzymatic reaction without rate-limiting the overall reaction. The enzyme-catalyzed reverse reaction was assayed with the EnzChek™ Phosphate Assay Kit that used purine nucleoside phosphorylase (PNP) to convert 2-amino-6-mercapto-7-methylpurine riboside (MESG) and the released phosphate ion to ribose 1-phosphate and 2-amino-6-mercapto-7-methylpurine, the latter of which could be monitored by its specific UV absorbance at 360 nm with an extinction coefficient of 11,000 M⁻¹ cm⁻¹.^[46] The assay was performed in

FULL PAPER

200 μ l solution containing 5 nM PlsX, 200 μ M MESH, 1 unit of PNP, 1 mM $MgCl_2$, and *holo*-ACP and palmitoyl phosphate at varied concentrations in 50 mM Tris pH 7.5. The reaction was also initiated by addition of the enzyme and monitored at 360 nm by a UV-VIS spectrometer (Shimadzu). Again, the coupling reaction was carefully tested not to limit the overall reaction. All assay experiments were performed in triplicate at 25 °C and the rate data were fitted with the Michaelis-Menten equation using GraphPad Prism 5.

Table 3. Oligodeoxyribonucleotide primers.

Name	Sequence
K184A-1	CGTCAGTTCGTTTCCTGCTTTATCTTCTGTTCCGACATTTA AAAGTCCG
K184A-2	CGGACTTTTAAATGTCGGAACAGAAGATAAAGCAGGAAAC GAACTGACG
K184Q-1	TCGTCAGTTCGTTTCCTGCTTTATCTTCTGTTCCGACATTTA AAAGTCCG
K184Q-2	CGGACTTTTAAATGTCGGAACAGAAGATAAAGCAGGAAAC GAACTGACG
K184R-1	CGTCAGTTCGTTTCCTCTTTTATCTTCTGTTCCGACATTTAA AAGTCC
K184R-2	GGACTTTTAAATGTCGGAACAGAAGATAAAGAGGAAACG AACTGACG
N229A-1	CAGCGTTTTGAGTGTAACAGCCCCGTAAGCCGCTCTGTT
N229A-2	AACAGACGGCTTTACCGGGGCTGTACTACTCAAACGCTG
N229Q-1	CAGCGTTTTGAGTGTAACCTGCCCGTAAGCCGCTCTGT
N229Q-2	ACAGACGGCTTTACCGGGCAGTTACTACTCAAACGCTG
R73A-1	GATGAGTTCCTTTTTCTTGCCACGGCAGGACCGGTT
R73A-2	AACCGGTCCGTGCCGTGGCAAGAAAAAGAACTCATC
R114A-1	GACGGTCAATTCCTTTAATTGCCCGACAATAAAGAGACCG GG
R114A-2	CCGGTCTCTTTATTGTCGGGGCAATTAAGGAATTGACCG TC
R120A-1	GAGCAAGCGCCGGAGCGTCAATTCCTTTAATTCTCC
R120A-2	GGAGAATTAAGGAATTGACGCTCCGGCGCTTGCTC
E181A-1	CAGTTCGTTTCCTTTTTATCTGCTGTTCCGACATTTAAAAG TCC
E181A-2	GGACTTTTAAATGTCGGAACAGCAGATAAAAAAGGAAACG AACTG
E209A-1	CTAAAAGGTCTCGCGCTGCCACGTTTCCGATAAAA
E209A-2	TTTTATCGGAAACGTGGCAGCGGAGACCTTTTAG
K233A-1	CAGAGCCTCCAGCGTTGCGAGTGAACATTCCCGG
K233A-2	CCGGGAATGTTACTACTCGCAACGCTGGAAGGCTCTG
E236A-1	GACAACGCAGACCTGCCAGCGTTTTGAGTG
E236A-2	CACTCAAACGCTGGCAGGCTCTGCGTTGTC

Structural analysis, sequence alignment and docking simulation. PyMOL version 1.3^[47] was used to perform structural analysis of the protein crystal structures and to generate all graphics. The protein interfaces were analyzed and the quaternary structure was determined using PISA,^[48] while the electrostatic potential surface was calculated using PDB2PQR plus APBS.^[49] Reviewed PlsX or Pta orthologues from UniProt^[50] were clustered with a 50% sequence identity and were aligned and analyzed by Clustal Omega.^[51] The alignment was presented with the *Bacillus subtilis* PlsX crystal structure (PDB ID: 6A1K) using ESPript 3.0.^[52]

Docking of small molecule ligands to the crystal structure of PlsX from *Bacillus subtilis* (PDB ID: 6A1K) was performed with Autodock (4.2.6) and the graphical user interface AutoDockTools (1.5.6).^[24] The ligands palmitoyl-phosphate, palmitoyl 4'-phosphopantetheinyl thioester or others were created by the online SMILES translator and structure file generator and optimized by eLBOW in Phenix software suite.^[53] The grid box was centered near the interface of the PlsX dimer and set to 100 spots in each dimension with a spacing of 0.3 Å. The Genetic Algorithm was chosen for the docking calculation process with its run number set to 25 and with a population size of 150. All other parameters were set to their default values. The docking results were visualized by AutoDockTools (1.5.6.) and the structure with the lowest binding energy was selected for analysis.

Acknowledgements

This work was financially supported by National Natural Science Foundation of China (Grant 21877094) and the Hong Kong Branch of Guangdong Southern Marine Science and Engineering Laboratory (Guangzhou) (Grant SMSEGL20SC01-E).

Keywords: phosphatidic acid biosynthesis • phosphate acyltransferase • active site • substrate recognition • enzyme mechanism

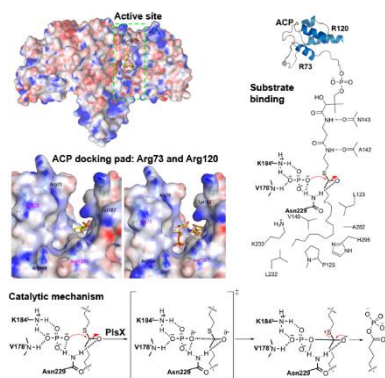
- [1] S. W. White, J. Zheng, Y. M. Zhang, C. O. Rock CO, *Annu. Rev. Biochem.* **2005**, *74*, 791-831.
- [2] Y.-J. Lu, Y. M. Zhang, K. D. Grimes, J. Qi, R. E. Lee, C. O. Rock, *Mol. Cell* **2006**, *23*, 765-772.
- [3] J. Yao, C. O. Rock, *Biochim. Biophys. Acta* **2013**, *1831*, 495-502.
- [4] Y.-M. Zhang, C. O. Rock, *J. Lipid Res.* **2008**, *49*, 1867-1874.
- [5] L. Paoletti, Y.-J. Lu, G. E. Schujman, D. de Mendoza, C. O. Rock, *J. Bacteriol.* **2007**, *189*, 5816-5824.
- [6] H. Takada, S. Fukushima-Tanaka, M. Morita, Y. Kasahara, S. Watanabe, T. Chibazakura, H. Hara, K. Matsumoto, H. Yoshikawa, *Mol. Microbiol.* **2014**, *91*, 242-255.
- [7] D. E. Sastre, A. Bisson-Filho, D. de Mendoza, F. J. Gueiros-Filho, *Mol. Microbiol.* **2016**, *100*, 621-634.
- [8] A. Müllera, M. Wenzel, H. Strahl, F. Grein, T. N. V. Saaki, B. Kohl, T. Siersma, J. E. Bandow, H.-G. Sahl, T. Schneider, L. W. Hamoen, *Proc. Natl. Acad. Sci. USA* **2016**, *113*, E7077-E7086.
- [9] H. Strahl, F. Bürmann, L. W. Hamoen, *Nat. Commun.* **2014**, *5*, 3442.
- [10] Y. P. Jiang, X. Dai, M. M. Qin, Z. Guo, *Commun. Biol.* **2019**, *2*, 316.
- [11] D. E. Sastre, L. G. M. Basso, B. Trastoy, J. O. Cifuentes, X. Contreras, F. Gueiros-Filho, D. de Mendoza, M. V. A. S. Navarro, M. E. Guerin, *J. Biol. Chem.* **2019**, Online first paper, doi: 10.1074/jbc.RA119.011122.
- [12] S. A. Kyrtopoulos, D. P. Satchell, *Biochim. Biophys. Acta* **1972**, *276*, 383-391.
- [13] R. A. Pelroy, H. R. Whiteley, *J. Bacteriol.* **1972**, *111*, 47-55.
- [14] J. Henkin, R. H. Abeles, *Biochemistry* **1976**, *15*, 3472-3479.
- [15] M. E. Rasche, K. S. Smith, J. G. Ferry, *J. Bacteriol.* **1997**, *179*, 7712-7717.
- [16] P. P. Iyer, J. G. Ferry, *J. Bacteriol.* **2001**, *183*, 4244-4250.
- [17] P. P. Iyer, S. H. Lawrence, K. B. Luther, K. R. Rajashankar, H. P. Yennawar, J. G. Ferry, H. Schindelin, *Structure* **2004**, *12*, 559-567.
- [18] S. H. Lawrence, K. B. Luther, H. Schindelin, J. G. Ferry, *J. Bacteriol.* **2006**, *188*, 1143-1154.

FULL PAPER

- [19] Q. S. Xu, J. Jancarik, Y. Lou, K. Kuznetsova, A. F. Yakunin, H. Yokota, P. Adams, R. Kim, S.-H. Kim, *J. Struct. Funct. Genomics* **2005**, *6*, 269–279.
- [20] J. Badger, J. M. Sauder, J. M. Adams, S. Antonysamy, K. Bain, M. G. Bergseid, S. G. Buchanan, M. D. Buchanan, Y. Batiyenko, J. A. Christopher, S. Emtage, A. Eroshkina, I. Feil, E. B. Furlong, K. S. Gajiwala, X. Gao, D. He, J. Hendle, A. Huber, K. Hoda, P. Kearins, C. Kissinger, B. Laubert, H. A. Lewis, J. Lin, K. Loomis, D. Lorimer, G. Louie, M. Maletic, C. D. Marsh, I. Miller, J. Molinari, H. J. Muller-Dieckmann, J. M. Newman, B. W. Noland, B. Pagarigan, F. Park, T. S. Peat, K. W. Post, S. Radojicic, A. Ramos, R. Romero, M. E. Rutter, W. E. Sanderson, K. D. Schwinn, J. Tresser, J. Winhoven, T. A. Wright, L. Wu, J. Xu J, T. J. R. Harris, *Proteins: Struct. Funct. Bioinform.* **2005**, *60*, 787-796.
- [21] Y. Kim, H. Li, T. A. Binkowski, D. Holzle, A. Joachimiak, *J. Struct. Funct. Genomics* **2009**, *10*, 157-163.
- [22] L. Holm, L. M. Laakso, *Nucleic acids Res.* **2016**, *44*, W351-W355.
- [23] J. E. Cronan, J. Thomas J, *Methods Enzymol.* **2009**, *459*, 395-433.
- [24] G. M. Morris, R. Huey, W. Lindstrom, M. F. Sanner, R. K. Belew, D. S. Goodsell, A. J. Olson, *J. Comput. Chem.* **2009**, *30*, 2785-2791.
- [25] Y.-M. Zhang, H. Marrakchi, S. W. White, C. O. Rock, *J. Lipid Res.* **2003**, *44*, 1-10.
- [26] Y.-M. Zhang, M. S. Rao, R. J. Heath, A. C. Price, A. J. Olson, C. O. Rock, S. W. White, *J. Biol. Chem.* **2001**, *276*, 8231-8238.
- [27] Y.-M. Zhang, B. Wu, J. Zheng, C. O. Rock, *J. Biol. Chem.* **2003**, *278*, 52935–52943.
- [28] V. Agarwal, S. Lin, T. Lukk, S. K. Nair, J. E. Cronan, *Proc Natl Acad Sci U S A* **2012**, *109*, 17406-17411.
- [29] J. Shi, X. Cao, Y. Chen, J. E. Cronan, Z. Guo, *Biochemistry* **2016**, *55*, 6705-6717.
- [30] A. Röttig, A. Steinbüchel *Microbiol. Mol. Biol. Rev.* **2013**, *77*, 277-321.
- [31] A. L. Lehninger, *J. Biol. Chem.* **1946**, *162*, 333-342.
- [32] Y. Lapidot, S. Rappoport, Y. Wolman, *J. Lipid Res.* **1967**, *8*, 142-145.
- [33] A. Al-Arif, M. Blecher, *J. Lipid Res.* **1969**, *10*, 344-345.
- [34] H. Schulz, *J. Biol. Chem.* **1974**, *249*, 2704-2709.
- [35] J. Knudsen, S. Clark, R. Dils, *Biochem. J.* **1976**, *160*, 683-691.
- [36] C. O. Rock, J. E. Cronan, I. M. Armitage, *J. Biol. Chem.* **1981**, *256*, 2669-2674.
- [37] D. Post-Beittenmiller, J. G. Jaworski, J. B. Ohlrogge, *J. Biol. Chem.* **1991**, *266*, 1858-1865.
- [38] M. A. de la Roche, Z. Shen, D. M. Byers, *Arch. Biochem. Biophys.* **1997**, *344*, 159–164.
- [39] H. Summer, R. Grämer, P. Dröge, *JoVE* **2009**, *32*, e1485.
- [40] Z.-F. Guo, Y. Sun, S. Zheng, Z. Guo, *Biochemistry* **2009**, *48*, 1712-1722.
- [41] Z.-F. Guo, M. Jiang, S. Zheng, Z. Guo, *Bioorg. Med. Chem. Lett.* **2010**, *20*, 3855-3858.
- [42] Y. Zou, J. Yin, *J. Am. Chem. Soc.* **2009**, *131*, 7548-7549.
- [43] E. Gasteiger, C. Hoogland, A. Gattiker, S. Duvaud, M. R. Wilkins, R. D. Appel, A. Bairoch, In *The Proteomics Protocols Handbook* (Ed.: J. M. Walker), *Humana Press*, **2005**, pp. 571–607.
- [44] G. L. Ellman, *Arch. Biochem. Biophys.* **1959**, *82*, 70-77.
- [45] P. W. Riddles, R. L. Blakeley, B. Zerner, *Anal. Biochem.* **1979**, *94*, 75-81.
- [46] M. R. Webb, *Proc. Natl. Acad. Sci. U S A* **1992**, *89*, 4884-4887.
- [47] W. L. DeLano In *DeLano Scientific*, San Carlos, CA, **2002**.
- [48] E. Krissinel, K. Henrick, *J. Mol. Biol.* **2007**, *372*, 774-797.
- [49] T. J. Dolinsky, J. E. Nielsen, J. A. McCammon, N. A. Baker, *Nucleic Acids Res.* **2004**, *32*, W665-W667.
- [50] The UniProt Consortium. *Nucleic Acids Res.* **2019**, *47*, D506-D515.
- [51] F. Sievers, A. Wilm, D. Dineen, T. J. Gibson, K. Karplus, W. Z. Li, R. Lopez, H. McWilliam, M. Remmert, J. Soding, J. D. Thompson, D. G. Higgins, *Mol. Syst. Biol.* **2011**, *7*, 539.
- [52] X. Robert, P. Gouet, *Nucleic Acids Res.* **2014**, *42*, W320-W324.
- [53] N. W. Moriarty, R. W. Grosse-Kunstleve, P. D. Adams, *Acta Crystallogr. Sect. D Biol. Crystallogr.* **2009**, *65*, 1074-1080.

FULL PAPER

Entry for the Table of Contents



The peripheral phosphate acyltransferase PlsX is shown to have an active site architecture different from phosphotransacetylases and to catalyze a similar acyl transfer reaction through a different mechanism. The catalysis likely involves substrate activation and transition state stabilization by two conserved residues, a lysine and an asparagine.